Cloud masking of SeaWiFS images over coastal waters using spectral variability.

K. Nordkvist, Hubert Loisel, Lucile Duforêt-Gaurier

Cloud masking of SeaWiFS images over coastal waters using spectral variability

Karin Nordkvist,[1,2,3,*] Hubert Loisel,[1,2,3] and Lucile Duforêt Gaurier[1,2,3]

[1]*Univ Lille Nord de France*
[2]*ULCO, LOG, F-62930 Wimereux, France*
[3]*CNRS, UMR 8187, F-62930 Wimereux, France*
[*]*Corresponding author: karin.nordkvist@univ-littoral.fr*

Abstract: Cloud masks developed in the frame of ocean color missions are usually based on the assumption that the marine reflectance is close to zero in the near-infrared (NIR). This is valid over the open ocean, but coastal (Case-2) waters may have a higher NIR reflectance due to suspended matter and non-maritime aerosols. Cloud-free pixels are sometimes classed as clouds, leading to a loss of data. We present an algorithm, based on standard ocean color wavelengths, that makes use of the lower spectral variability of clouds compared to water. Images from different coastal areas have been used to develop and test the algorithm and a radiative transfer model has been used for a numerical sensitivity analysis. The algorithm shows a good performance in many of the tested scenes, and using this algorithm instead of the standard SeaWiFS NIR threshold will increase the amount of data over Case-2 waters.

OCIS codes: (010.0280) Remote sensing and sensors; (280.4991) Passive remote sensing; (010.4450) Ocean optics; (010.1615) Clouds

References and links

1. W. D. Robinson, B. A. Franz, F. S. Patt, S. W. Bailey, and P. J. Werdell, "Masks and flags updates," in *NASA Technical Memorandum*, S. B. Hooker and E. R. Firestone, eds., Vol. **22**, pp. 34-40 (2003).
2. G. C. Feldman and C. R. McClain, "Ocean Color Web, SeaWiFS Reprocessing 5.2," NASA Goddard Space Flight Center, N. Kuring and S. W. Bailey, eds., http://oceancolor.gsfc.nasa.gov.
3. R. P. Stumpf, R. A. Arnone, R. W. Gould, P. M. Martinolich, and V. Ransibrahmanakul, "A partially coupled ocean-atmosphere model for retrieval of water-leaving radiance from SeaWiFS in coastal waters," in *NASA Technical Memorandum*, S. B. Hooker and E. R. Firestone, eds., Vol. 22, pp. 51-59 (2003).
4. M. Wang and W. Shi, "Cloud masking for ocean color data processing in the coastal regions," IEEE Trans. Geosci. Remote Sens. **44**, 3196-3205 (2006).
5. R. Frouin, P.-Y. Deschamps, J.-M. Nicolas, and P. Dubuisson, "Ocean color remote sensing through clouds," Proc. SPIE **5885**, 588504 (2005).
6. D. Nobileau and D. Antoine, "Detection of blue-absorbing aerosols using near infrared and visible (ocean color) remote sensing observations," Remote Sens. Environ. **95**, 368-387 (2005).
7. J.-M. Nicolas, P.-Y. Deschamps, H. Loisel, and C. Moulin, "Algorithm Theoretical Basis Document, POLDER-2 / Ocean Color / Atmospheric corrections," http://smsc.cnes.fr/POLDER/A_produits_scie.htm.
8. H. R. Gordon, "Atmospheric correction of ocean color imagery in the Earth Observing System era," J. Geophys. Res. **102**, 17 081-17 106 (1997).
9. M. Wang and S. W. Bailey, "Correction of sun glint contamination on the SeaWiFS ocean and atmosphere products," Appl. Opt. **40**, 4790-4798 (2001).
10. K. D. Moore, K. J. Voss, and H. R. Gordon, "Spectral reflectance of whitecaps: Their contribution to water-leaving radiance," J. Geophys. Res. **105**, 6493-6499 (2000).
11. J.-M. Nicolas, P.-Y. Deschamps, and R. Frouin, "Spectral reflectance of oceanic whitecaps in the visible and near infrared: Aircraft measurements over open ocean," Geophys. Res. Lett. **28**, 4445-4448 (2001).
12. M. Wang, "Validation study of the SeaWiFS oxygen A-band absorption correction: comparing the retrieved cloud optical thickness from SeaWiFS measurements," Appl. Opt. **38**, 937-944 (1999).
13. J. V. Martins, D. Tanré, L. Remer, Y. Kaufman, S. Mattoo, and R. Levy, "MODIS cloud screening for remote sensing of aerosols over oceans using spatial variability," Geophys. Res. Lett. **29**, 10.1029 /2001GL013252 (2002).

#107421 - $15.00 USD Received 10 Feb 2009; revised 8 May 2009; accepted 19 May 2009; published 6 Jul 2009

14. B. Lubac and H. Loisel, "Variability and classification of remote sensing reflectance spectra in the eastern English Channel and southern North Sea," Remote Sens. Environ. **110**, 45-58 (2007).
15. L. Duforêt, R. Frouin, and P. Dubuisson, "Importance and estimation of aerosol vertical structure in satellite ocean-color remote sensing," Appl. Opt. **46**, 1107-1119 (2007).
16. G. L. Stephens, *Optical properties of eight water cloud types*, Aust. Div. Atmos. Phys. Tech. Pap.**,** (CSIRO, Melbourne, 1979) Vol. 36 .
17. D. Doxaran, J.-M. Froidefond, S. Lavender, and P. Castaing, "Spectral signature of highly turbid waters. Application with SPOT data to quantify suspended particulate matter concentrations," Remote Sens. Environ. **81**, 149-161 (2002).
18. H. Loisel and A. Morel, "Non-isotropy of the upward radiance field in typical coastal (Case 2) waters," Int. J. Remote Sens. **22**, 275-295 (2001).
19. K. Ruddick, F. Ovidio, and M. Rijkeboer, "Atmospheric correction of SeaWiFS imagery for turbid coastal and inland waters," Appl. Opt. **39**, 897-912 (2000).
20. J.-M. Froidefond, F. Lahet, C. Hu, D. Doxaran, D. Guiral, M. T. Prost, and J.-F. Ternon, "Mudflats and mud suspension observed from satellite data in French Guiana," Mar. Geol. **208**, 153-168 (2004).
21. T. Iida, S. I. Saitoh, T. Miyamura, M. Toratani, H. Fukushima, and N. Shiga, "Temporal and spatial variability of coccolithophore blooms in the eastern Bering Sea," Prog. Oceanogr. **55**, 165-175 (2002).
22. S. Chen, G. Zhang, and S. Yang, "Temporal and spatial changes of suspended sediment concentration and resuspension in the Yangtze River estuary," J. Geog. Sci. **13**, 498-506 (2003).
23. H. Loisel, X. Meriaux, J.-F. Berthon, and A. Poteau, "Investigation of the optical backscattering to scattering ratio of marine particles in relation to their biogeochemical composition in the eastern English Channel and southern North Sea," Limnol. Oceanogr. **52**, 739-752 (2007).
24. R.-R. Li, Y. J. Kaufman, B.-C. Gao, and C. O. Davis, "Remote sensing of suspended matter and shallow coastal waters," IEEE Trans. Geosci. Remote Sens. **41**, 559-566 (2003).

1. Introduction

Ocean color retrieval by satellite borne sensors is in principle only possible for a clear (cloud-free) atmosphere, and cloud-contaminated pixels have to be removed from the images before any ocean color processing takes place. The cloud masks developed in the frame of ocean color missions are based on the assumption that the marine reflectance in the near-infrared (NIR) is equal or close to zero. In the processing of images acquired by the Sea-viewing Wide Field-of-view Sensor (SeaWiFS) and the Moderate Resolution Imaging Spectrometer (MODIS), a threshold at the 865 nm (SeaWiFS) and 869 nm (MODIS) surface reflectance is used to distinguish between clouds and water [1, 2]. This generally works well in the open ocean, which can adequately be considered as black in the NIR (except in the presence of intense coccolithophore blooms). In turbid coastal waters however, a higher concentration of suspended particles can give a significant reflectance in these wavelengths [3]. Non-maritime aerosols like dust and smoke may also cause a high NIR reflectance [4]. Cloud-free pixels are then sometimes classed as clouds and excluded from further processing, leading to a loss of data in these areas. Frouin *et al.* [5] have shown that the marine reflectance can be estimated in the presence of a thin or broken cloud layer, but the method requires a negligible marine reflectance in the NIR.

Different algorithms have been developed to mask clouds while keeping areas with turbid water or aerosols for further processing [4, 6, 7]. These algorithms differ by their inherent assumptions and the wavelengths used. For example, Wang and Shi [4] present an algorithm that makes use of the fact that even turbid waters have a very low reflectance in the shortwave infrared (SWIR) wavelengths. They also present a second algorithm intended to be used with sensors that do not have SWIR bands. It is built on the assumption that the spectral variability in the NIR is lower for clouds than for water. Nobileau and Antoine [6] developed a method to mask clouds while leaving dust plumes for further processing. A threshold in 412 nm is used since dust aerosols absorb more in the blue than clouds do. Water is spatially more homogeneous than clouds, and the cloud mask for the POLarization and Directionality of the Earth's Reflectances (POLDER) sensor uses a threshold on the spatial variability in 865 nm [7]. The present study tests the performance of these algorithms in different types of water and in different geographical areas. We also present an algorithm for cloud screening of SeaWiFS images, aiming to work for different types of turbid Case-2 waters. This algorithm makes use

#107421 - $15.00 USD Received 10 Feb 2009; revised 8 May 2009; accepted 19 May 2009; published 6 Jul 2009

of the fact that clouds are spectrally relatively flat compared to turbid waters and aerosols [4, 5].

First, some general equations, different algorithms and a radiative transfer code used for numerical simulations are presented together with a description of our algorithm. Then an intercomparison of the performance of the different algorithms in various scenes is presented. At last a sensitivity analysis is conducted to assess the effect of varying cloud optical thickness and altitude on the performance of our algorithm.

2. Method

2.1 General equations

For a cloud-free atmosphere over ocean, the top-of-the-atmosphere (TOA) reflectance, ρ_{TOA}, at a given wavelength, λ, received by the satellite sensor can be written as

$$\rho_{TOA}(\lambda)=\rho_{path}(\lambda)+T(\lambda)\rho_g(\lambda)+t(\lambda)\rho_{wc}(\lambda)+t(\lambda)\rho_w(\lambda) \quad (1)$$

[8], where $\rho_g(\lambda)$ is the sun glint reflectance [9], $\rho_{wc}(\lambda)$ the reflectance from whitecaps [10] and $\rho_w(\lambda)$ the marine reflectance. Sun glint and whitecap contributions can be modeled using wind speed and geometry, but for simplicity they are neglected in the following discussion. The SeaWiFS sensor can be tilted away from the glint pattern, but the whitecap reflectance has a non negligible effect on the remotely sensed signal. Studies conducted by Moore et al. and Nicolas et al., among others, have shown that it is spectrally dependent and decreases with wavelength [10, 11]. The effects of ignoring the whitecap reflectance in the cloud mask algorithm should be studied specially for high wind speeds. $T(\lambda)$ and $t(\lambda)$ are the direct and diffuse transmittances of the atmosphere, respectively. The path reflectance $\rho_{path}(\lambda)$ is defined as

$$\rho_{path}(\lambda)=\rho_r(\lambda)+\rho_a(\lambda)+\rho_{ra}(\lambda). \quad (2)$$

Here $\rho_r(\lambda)$ is the reflectance due to Rayleigh scattering in a purely molecular atmosphere and $\rho_a(\lambda)$ is the reflectance resulting from multiple scattering by aerosols in a pure aerosol atmosphere. $\rho_{ra}(\lambda)$ represents the interaction between these processes in a real atmosphere containing both molecules and aerosols [8]. The interaction between cloud and aerosol scattering is neglected. The term $\rho_A(\lambda)$ is introduced as the sum of $\rho_a(\lambda)$ and $\rho_{ra}(\lambda)$. We then have

$$\rho_{TOA}(\lambda)=\rho_r(\lambda)+\rho_A(\lambda)+t(\lambda)\rho_w(\lambda). \quad (3)$$

In the presence of clouds, the TOA reflectance is

$$\rho_{TOA}(\lambda)=\rho_c(\lambda)+\rho_{rc}(\lambda)+\rho_r(\lambda)+\rho_A(\lambda)+t(\lambda)\rho_w(\lambda), \quad (4)$$

where $\rho_c(\lambda)$ is the cloud reflectance in a pure cloud atmosphere and $\rho_{rc}(\lambda)$ the interaction between cloud and Rayleigh scattering. The surface reflectance $\rho_s(\lambda)$ is a product of the SeaWiFS Level 2 processing and is calculated as

$$\rho_s = \frac{\pi}{F_0\mu_0}\left(\frac{L_{TOA}}{t_{g,sol}t_{g,sen}} - L_r\right)\Bigg/(t_{sol}t_{sen}t_{O_2}t_{H_2O}), \quad (5)$$

where F_0 is the mean solar irradiance, μ_0 the cosine of the solar zenith angle, L_{TOA} the TOA upwelling radiance and L_r the upwelling radiance due to Rayleigh scattering by molecules. The letter t is used for the different transmissions. Radiances and transmissions are wavelength dependent, but λ has been omitted from Eq. (5). Subscripts g, O_2 and H_2O denote transmission by gases, oxygen and water vapor, respectively. *sol* and *sen* stand for the paths sun-to-ground and ground-to-sensor. $\rho_s(\lambda)$ is thus the reflectance when all atmospheric corrections except for aerosols, sun glint and whitecaps have been done. Based on Eq. (3) for a cloud-free atmosphere, $\rho_s(\lambda)$ can be written as

#107421 - $15.00 USD Received 10 Feb 2009; revised 8 May 2009; accepted 19 May 2009; published 6 Jul 2009

$$\rho_s(\lambda)=\rho_{TOA}(\lambda)-\rho_r(\lambda)$$
$$=t(\lambda)\rho_w(\lambda)+\rho_A(\lambda). \quad (6)$$

The corresponding equation in the presence of clouds is

$$\rho_s(\lambda)=\rho_{TOA}(\lambda)-\rho_r(\lambda)$$
$$=t(\lambda)\rho_w(\lambda)+\rho_A(\lambda)+\rho_c(\lambda)+\rho_{rc}(\lambda). \quad (7)$$

2.2 Description of different algorithms

The standard SeaWiFS and MODIS cloud masking algorithm uses a threshold on the 865 nm (SeaWiFS) and 869 nm (MODIS) surface reflectance. It is assumed that the ocean is black in this region of the spectra so that any signal is of atmospheric origin, for example light scattered by aerosols and/or clouds. Pixels where $\rho_s(865)-\rho_g(865)>0.027$, whatever the geometry of observation, are masked as cloudy and are excluded from further ocean color processing [1,2]. $\rho_g(865)$ is the reflectance of directly transmitted sun glint.

Wang and Shi [4] describe an algorithm using the MODIS SWIR channels. This well performing algorithm can not be used with sensors that do not have SWIR bands, for example SeaWiFS. For such sensors, the authors propose a two-step algorithm that, in addition to the standard NIR threshold, makes use of the ratio between the Rayleigh-corrected reflectance in two NIR bands. The Rayleigh-corrected (RC) TOA reflectance is defined as

$$\Delta\rho^{(RC)}(\lambda)=\rho_{TOA}(\lambda)-\rho_r(\lambda), \quad (8)$$

and the ratio between the RC reflectance in two bands λ_i and λ_j as

$$\varepsilon^{(RC)}(\lambda_i,\lambda_j)=\Delta\rho^{(RC)}(\lambda_i)/\Delta\rho^{(RC)}(\lambda_j). \quad (9)$$

The algorithm was developed using MODIS data, with the 748 nm and 869 nm channels as λ_i and λ_j, respectively. In the first step, two thresholds in the NIR band are used to identify cloud-free pixels and to exclude the brightest clouds from further calculations. The atmosphere is considered as clear for cases with $\Delta\rho^{(RC)}(\lambda_j)\leq 0.027$ and cloudy if $\Delta\rho^{(RC)}(\lambda_j)>0.06$. In the second step the ratio $\varepsilon^{(RC)}(\lambda_i,\lambda_j)$ is calculated for pixels where $0.027<\Delta\rho^{(RC)}(\lambda_j)\leq 0.06$. If $\varepsilon^{(RC)}(\lambda_i,\lambda_j)$ exceeds or is equal to the threshold value 1.15 the atmosphere is identified as clear. In the tests with SeaWiFS images, the channels 765 and 865 nm are used. The 765 nm SeaWiFS channel, extending from 745 to 785 nm, encompasses the oxygen A-band at 762 nm. This is not the case for the MODIS 748 nm band. Absorption by oxygen will reduce the measured signal at 765 nm, and thus the ratio $\varepsilon^{(RC)}(765,865)$ [12]. A consequence of this is that water pixels that would be correctly identified in a MODIS image may be masked as clouds in a SeaWiFS image.

Nobileau and Antoine [6] present a method for identifying blue-absorbing aerosols in near-infrared and visible remote sensing observations. Their work includes an improved cloud mask applicable to the SeaWiFS and MERIS sensors, based on the fact that dust aerosols absorb in the blue part of the spectrum whereas clouds do not. Note that cloud screening over sediment-rich waters is not the main purpose of this algorithm. It was developed for aerosol applications, where clouds but not aerosols need to be masked out. As opposite to the SeaWiFS/MODIS NIR threshold and the method by Wang and Shi (2006), this algorithm uses the TOA reflectance $\rho_{TOA}(\lambda)$, which is not corrected for molecular scattering, since the interaction term $\rho_{rc}(\lambda)$ is unknown and can not be corrected for. A first threshold in the near-infrared, $\rho_{TOA}(865)>0.2$, is used to eliminate landmasses and the brightest clouds. Secondly, a threshold at the 412 nm band is used to mask less bright clouds. Due to the large Rayleigh contribution and significant coupling between molecular and aerosol scattering in the short visible wavelengths, the TOA signal in this part of the spectrum is dependent on the geometry of the observation and a geometry-dependent threshold is used. The threshold values were derived by simulating $\rho_{TOA}(\lambda)$ for an atmosphere with aerosols of high optical thickness, and a

#107421 - $15.00 USD Received 10 Feb 2009; revised 8 May 2009; accepted 19 May 2009; published 6 Jul 2009

three-dimensional lookup table with solar zenith angle, viewing zenith angle and azimuth difference as input was generated.

Clouds show a larger spatial variability than aerosols and sea water, which suggests the use of a spatial variability test for cloud screening. Such algorithms are used for MODIS aerosol retrieval over oceans [13] and for the POLDER and PARASOL cloud mask [7]. The latter two sensors have the ability to picture the same part of the ground in up to 14 (POLDER 1 and 2) and 16 (PARASOL) different angles in 9 spectral bands, 3 of which are associated with polarization filters. The spatial resolution is 6*7 km^2. The main test in the cloud mask is a threshold on the local standard deviation in the TOA reflectance at 865 nm, $\rho_{TOA}(865)$, applied to the viewing direction in which the 865 nm reflectance is smallest. The standard deviation in a 3*3 pixels box around each pixel is computed and pixels with a local standard deviation higher than 0.005 are considered as clouds. Coastal areas may be a problem for this algorithm since the spatial variability of $\rho_w(\lambda)$ is high [14].

2.3 Numerical simulations

The thinner the cloud, the more it reveals the spectral signature of the water, making thinner clouds more difficult to detect with our algorithm. Therefore the impact of the cloud optical thickness, τ, on $\rho_s(\lambda)$ will be tested through numerical simulations. A second set of simulations will be performed to assess the impact of the coupling term between molecular and cloud scattering, $\rho_{rc}(\lambda)$, which is neglected by most algorithms. When $\rho_s(\lambda)$ is estimated from a SeaWiFS image, the correction for molecular scattering is done for a cloud-free case. Thus, for the cloudy pixels, $\rho_{rc}(\lambda)$ is not corrected for, Eq. (7). $\rho_{rc}(\lambda)$ is a constructed term which is introduced to account for the fact that the contributions $\rho_r(\lambda)$ and $\rho_c(\lambda)$ from a purely molecular atmosphere and from a cloud, respectively, are not additive. $\rho_{rc}(\lambda)$ is more important at shorter wavelengths since the Rayleigh scattering varies as $\lambda^{-4.09}$. It is also affected by the molecular content at the level of the cloud and thus by the cloud altitude. At last, the effect of different viewing and illumination geometries on the performance of our algorithm will be tested.

In order to test the impact of varying cloud optical thickness and altitude on the ρ_s spectrum, simulations are made by GAMEAD (Global Atmospheric ModEl, Adding-Doubling), a radiative transfer model for the ocean-atmosphere system [15]. The code takes into account molecule and cloud scattering, cloud absorption and interactions between scattering and absorption. As the TOA reflectance is very sensitive to the lower boundary conditions, reflection of the atmospheric radiance field on the wavy sea surface must be accurately accounted for. The wavy-sea surface description is based on the Fresnel formula and on the Cox and Munk wave slope probability density. In our simulations, the wind speed is set to 5.0 m/s. First, simulations are performed for a cloud-free atmosphere, then in presence of a typical stratocumulus cloud (stratocumulus 1 model, [16]). Numerical simulations are carried out for different cloud optical thicknesses (1.0, 3.0 and 5.0 at 555 nm) and altitudes (0.5, 1.5 and 2.5 km). Cloud optical thicknesses of 1.0, 3.0 and 5.0 correspond to a plane albedo of 0.05, 0.17 and 0.27, respectively. The solar and sensor zenith angles, θ_s and θ_v, are kept at 30° and 0° respectively, except for in the directionality test where θ_s varies between 0° and 57° and θ_v between 0° and 55°. Radiative transfer within the water body is not simulated by the code, but a wavelength dependent albedo is used as input to the simulations in order to account for the marine reflectance. In our study case, a reflectance spectrum from the Gironde estuary in southwest France is used [17]. The total suspended matter (TSM) concentration was 180 mg/l at the time of the measurement. Note that it has been shown that the upward radiance field is not isotropic and remains sun-angle dependent even in turbid natural waters [18]. However, the isotropy increases with an increased particle concentration thanks to the higher number of scattering events. As the TSM concentration is high for the considered spectrum, we assume a Lambertian marine reflectance. Since $\rho_s(\lambda)$ is corrected for absorption by water vapor, oxygen and other gases, the gaseous absorption is not included in the simulations. Neither is the aerosol contribution, although $\rho_s(\lambda)$ contains this term, Eqs. (6) and (7).

#107421 - $15.00 USD Received 10 Feb 2009; revised 8 May 2009; accepted 19 May 2009; published 6 Jul 2009

The estimation of $\rho_s(\lambda)$ from the numerical simulations is done in two steps. A first simulation of $\rho_{TOA}(\lambda)$ is made using the marine reflectance. Then a second simulation is made for a cloud-free atmosphere with the marine reflectance $\rho_w(\lambda)$ set to zero. The result of this second simulation is then equal to the molecular scattering term $\rho_r(\lambda)$, and the surface reflectance is obtained by subtracting $\rho_r(\lambda)$ from $\rho_{TOA}(\lambda)$.

2.4 Algorithm

Even in very sediment-rich waters, where clear pixels are mistakenly masked as clouds by the current SeaWiFS algorithm, the human eye is often capable of discriminating between the two since the water is obviously "non-white". The proposed algorithm makes use of the low spectral variability of clouds compared to water. A first step uses the NIR threshold from the standard SeaWiFS and MODIS cloud masks to identify cloud-free pixels. The second step uses ρ_s at the spectral bands centered at 412, 555, 670 and 865 nm. Among these channels, the one with the maximum surface reflectance is denoted λ_{max} and the one with the minimum surface reflectance is denoted λ_{min}. The ratio ε_{max} is calculated as

$$\varepsilon_{max}=\rho_s(\lambda_{max})/\rho_s(\lambda_{min}), \tag{10}$$

so that a low spectral variability, typical for clouds, results in a low ε_{max} and vice versa. The choice of these channels is motivated by the shape of the ρ_w spectra encountered in coastal areas. In turbid waters, the maximum reflectance is normally located around 555 or 670 nm while the minimum reflectance generally occurs around 412 or 865 nm [14,19-21]. As we don't use the 765 nm channel, the oxygen absorption at 762 nm is not a problem. Tests show that when using all eight SeaWiFS channels (412, 443, 490, 510, 555, 670, 765 and 865 nm), and the same ε_{max} threshold as above, the number of pixels identified as water does not change.

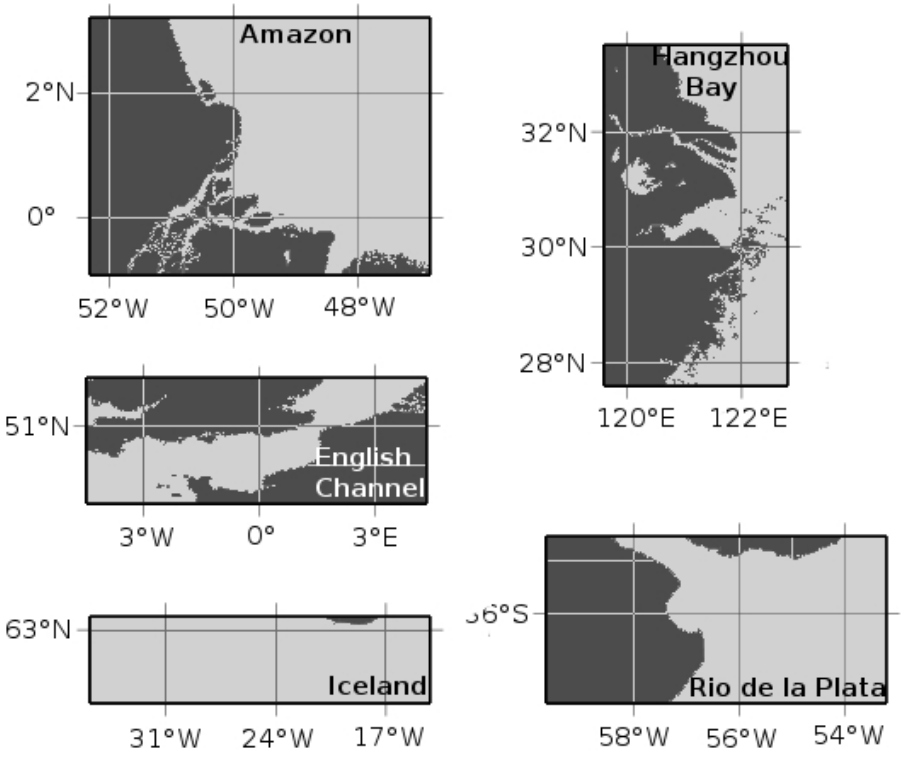

Fig. 1. Maps of the areas used to test and develop the algorithm.

#107421 - $15.00 USD Received 10 Feb 2009; revised 8 May 2009; accepted 19 May 2009; published 6 Jul 2009

A set of 200 training pixels from SeaWiFS images [2] from different regions has been used to examine the behavior of ρ_s and ε_{max} for cloudy and cloud-free pixels. A total of 20 scenes was used (table 1), and ten pixels, five cloudy and five cloud-free, were selected in each scene. These training pixels include clouds of different thicknesses and water that differ in terms of composition and thus optically significant properties. The regions are the Amazon estuary (A), the Rio de la Plata estuary (R), the area south of Iceland (I), the English Channel (E) and the Hangzhou Bay and Yellow Sea region (Y) (Fig. 1). These areas have been selected as typical turbid waters, covering a large range of variability in the properties of the suspended marine particles. The water in A and R is characterized by very high concentrations of suspended particulate matter (SPM) mainly originating from the rivers. This also holds for region Y, which permanently has very high SPM concentrations [21]. Region E with its high tidal range, strong tidal currents, relatively shallow water and freshwater discharges from different rivers also has a high content of inorganic and organic particles [22]. Scene I shows a large coccolithophore bloom that occurred south of Iceland in the summer of 1998. A scatter plot of $\rho_s(865)$ versus ε_{max} for the training pixels is shown in Fig. 2(a). Only cloud-free pixels have $\rho_s(865) \leq 0.027$ (threshold indicated by the dotted horizontal line), and these are correctly identified as water by the NIR test in the first step. Among the remaining pixels ($\rho_s(865) > 0.027$), one can see a clear trend with cloud pixels in the left part of the diagram (low ε_{max}) and cloud-free pixels in the right part (high ε_{max}). Tests with different threshold values and visual inspection of the results show that $\varepsilon_{max}=2.5$, indicated by the dotted vertical line, is a good threshold value for identifying clouds in the second step of the algorithm. Several color composites with different combinations of spectral bands were used in order to facilitate the interpretation of the result. A combination of the bands 865, 443 and 412 nm as red, green and blue appeared to be useful for the most turbid waters. If one skipped the first step and only used the ε_{max} threshold, some spectrally flat water pixels (see the lower left part of the plot) would be flagged as cloudy.

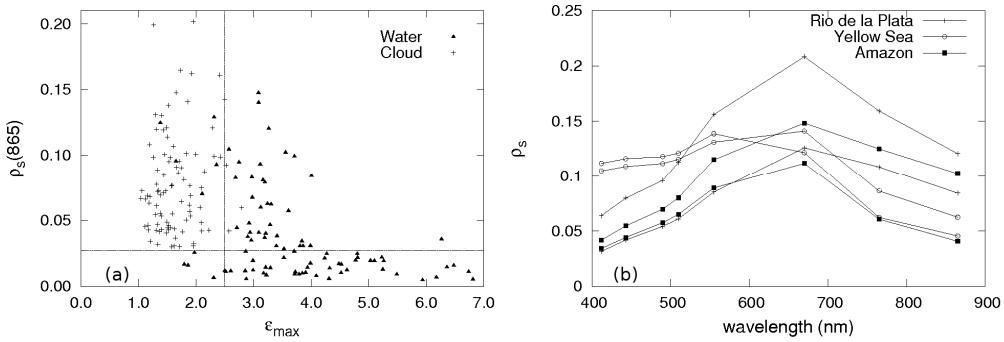

Fig. 2. (a). Scatter plot of $\rho_s(865)$ versus ε_{max} for several cloudy and cloud-free pixels, from the areas presented in Fig. 1. The chosen threshold values for $\rho_s(865)$ and ε_{max} are shown as dotted horizontal and vertical lines, respectively. (b) Examples of ρ_s spectra from SeaWiFS images of the Amazon and Rio de la Plata estuaries and the Yellow Sea. Each graph corresponds to one training pixel.

Figure 2(b) shows ρ_s spectra from a few of the training pixels. The Yellow Sea spectra are comparatively flat, with high reflectance values in the shorter wavelengths as well as in the NIR. The high reflectance in the blue region is most likely due to large amounts of pollution and dust aerosols [23], which together with the high SPM concentrations also contribute to the strong NIR reflectance. The five water pixels in the upper left part of the scatter plot in Fig. 2(a) all come from this area, which in a MODIS image from the same day was found to be cloud-free by the SWIR algorithm by Wang and Shi [4]. If one uses our algorithm with the

#107421 - $15.00 USD Received 10 Feb 2009; revised 8 May 2009; accepted 19 May 2009; published 6 Jul 2009

threshold value proposed here, ε_{max}=2.5, these pixels will be classed as clouds. Some of the cloud pixels from the Amazon and Rio de la Plata estuaries are very close to the ε_{max} threshold, some above it and some below. A closer look at the images shows that these pixels are located in areas with a thin or broken cloud cover and often very turbid water, and that they are difficult to identify by visual examination. One possible way to deal with these cases is to define a narrow interval around the ε_{max} threshold, and to introduce a third "unidentified or mixed" class for pixels within this interval.

3. Results

3.1 Intercomparison of the algorithm performances

The four cloud masks described above have been tested on several scenes from the five regions presented in Fig. 1. Figures 3-7 show SeaWiFS images of a few scenes and the different algorithms applied to each of them. The fixed NIR threshold efficiently masks the clouds, but also masks much of the turbid waters in scenes A5 (Fig. 3(b)), R4 (Fig. 4(b)) and Y2 (Fig. 5(b)). To test the algorithm by Wang and Shi [4], SeaWiFS bands at 865 and 765 nm are used. This algorithm works better than the fixed NIR threshold in scenes A5 (Fig. 3(c)), R4 (Fig. 4(c)) and Y2 (Fig. 5(c)), but still masks some of the cloud-free areas, for example north of the Amazon estuary. Both the fixed NIR threshold and the algorithm by Wang and Shi work well in scene I1 (Figs. 7(b), 7c)). The method by Nobileau and Antoine [6] works relatively well in scenes A5 (Fig. 3(d)) and R4 (Fig. 4(d)), but misses some thinner clouds in R4 and masks some of the water in A5. It masks parts of the coccolithophore bloom in scene I1 (Fig. 7(d)) and some of the turbid waters in scene E6 (Fig. 6(d)). Note however that this cloud mask was developed for aerosol applications, not for cloud detection over turbid waters. The threshold value of 0.005 on the ρ_{TOA}(865) spatial variability in the POLDER algorithm is too low when this method is used on the SeaWiFS images, and many cloud-free areas are masked (result not shown). Figures 3-7 show the result when this threshold has been adjusted to 0.01, which works relatively well in scenes A5 (Fig. 3(e)), R4 (Fig. 4(e)) and Y2 (Fig. 5(e)) but results in undetected clouds in scenes I1 (Fig. 7(e)) and E6 (Fig. 6(e)). The sharp edges between waters of different brightness are masked in scenes A5 and R4. Worth mentioning is that this is the only algorithm that, when properly tuned, does not mask the entire Hangzhou Bay (Fig. 5(e)). The latter two methods are computationally heavier than the other algorithms.

Our algorithm shows a good overall performance in many of the selected scenes and recovers water pixels that are masked as clouds by other algorithms. It misses some of the thinner clouds in scene I1 (Fig. 7(f)) and probably also in A5 (Fig. 3(f)). The biggest difficulties are encountered in scene Y2 (Fig. 5(f)), where the entire Hangzhou Bay is masked, most probably due to a high aerosol optical thickness. As mentioned in Sec. 2.4, the reflectance spectrum in region Y is relatively flat with high values both in the blue and in the NIR part.

A large range of solar (6°-75°) and viewing (22°-57°) zenith angles is covered by the tested scenes. The solar and sensor zenith angles, θ_s and θ_v, are examined for the most difficult cases: pixels close to the ε_{max} threshold and cloud masked water pixels from the Yellow Sea. Among these, only the pixels from scene Y2 have potentially problematic illumination and viewing geometries, with θ_s and θ_v around 57° and 55° respectively. Their ε_{max} ratio is 10 – 40% lower than the threshold value of 2.5. Numerical simulations as described in Sec. 2.3 show that ε_{max} actually increases (3.4%) for this geometry, compared to a case with θ_s=30° and θ_v=0°, which emphasizes that directionality effects are not the reason why these pixels are mistakenly masked as clouds.

#107421 - $15.00 USD Received 10 Feb 2009; revised 8 May 2009; accepted 19 May 2009; published 6 Jul 2009

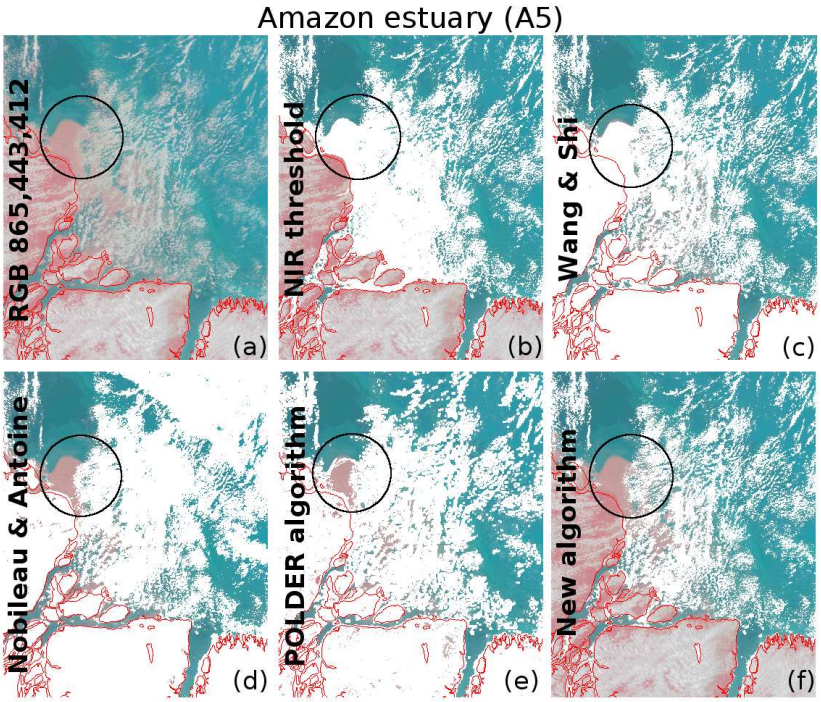

Fig. 3. A SeaWiFS image of scene A5 in table 1, with (a) no cloud mask and (b-f) the different cloud masks applied. The color composite has the 865, 443 and 412 nm channels as red, green and blue, respectively. Areas of special interest are indicated with black circles.

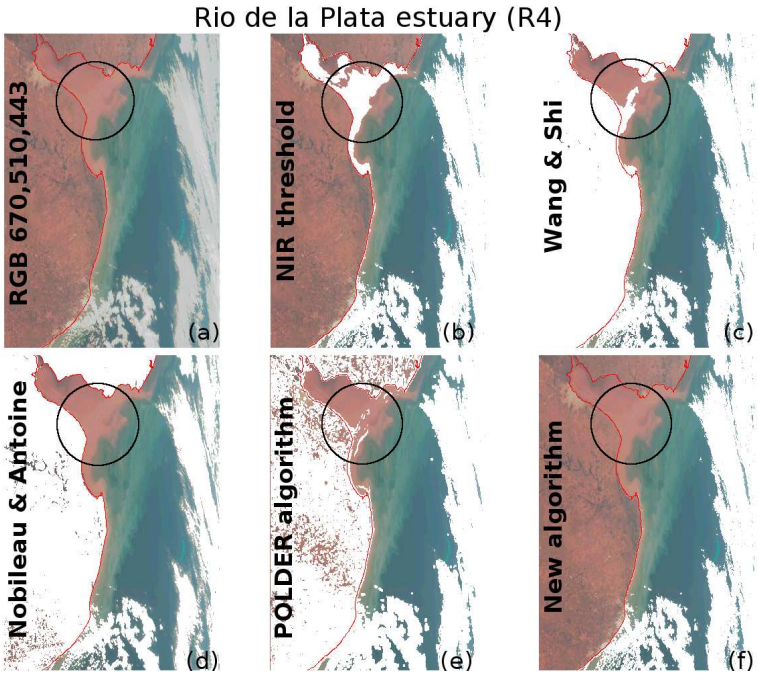

Fig. 4. As Fig. 3 but for scene R4. The color composite has the 670, 510 and 443 nm channels as red, green and blue.

#107421 - $15.00 USD Received 10 Feb 2009; revised 8 May 2009; accepted 19 May 2009; published 6 Jul 2009

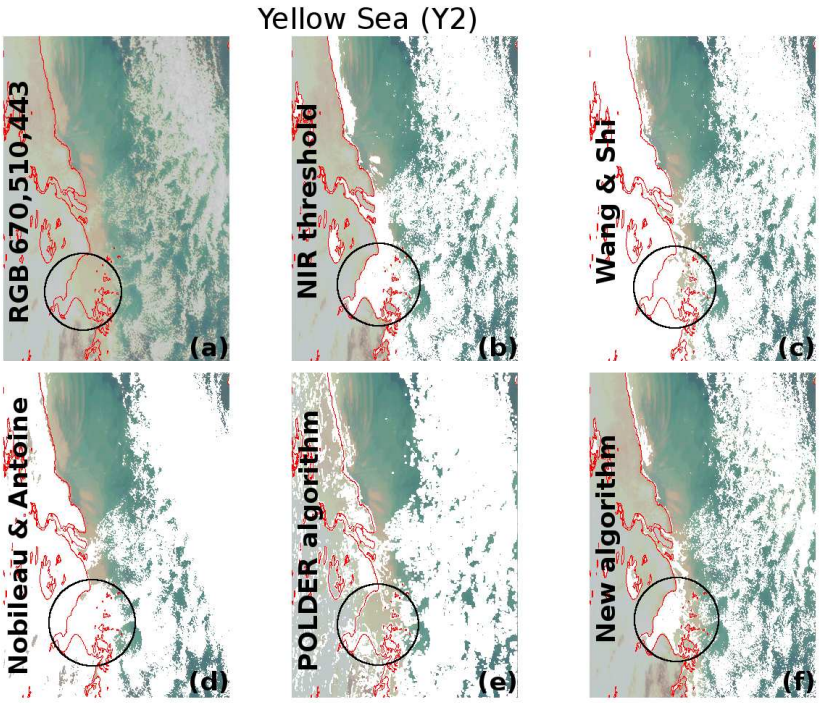

Fig. 5. As Fig. 4 but for scene Y2.

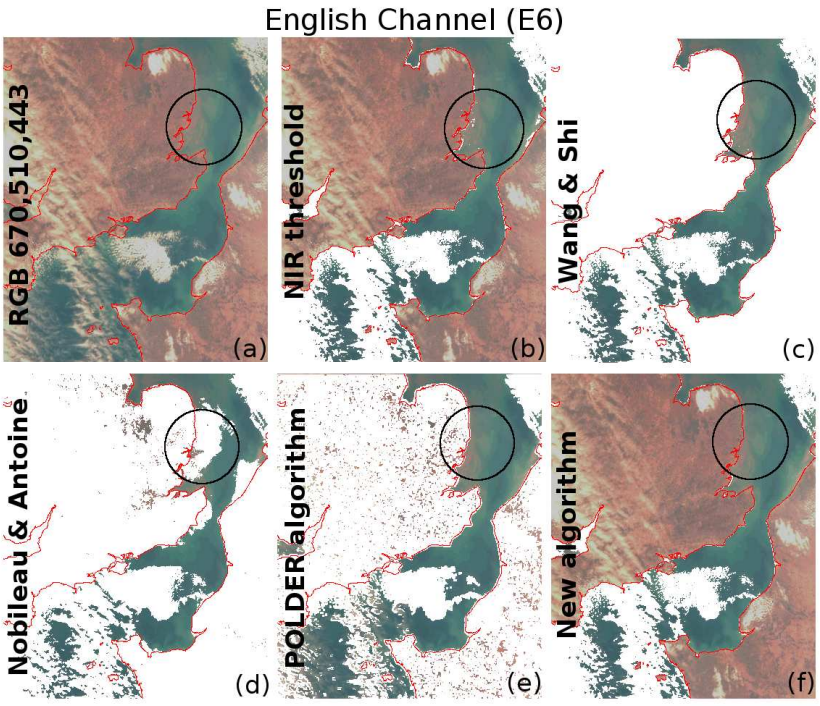

Fig. 6. As Fig. 4 but for scene E6.

#107421 - $15.00 USD Received 10 Feb 2009; revised 8 May 2009; accepted 19 May 2009; published 6 Jul 2009

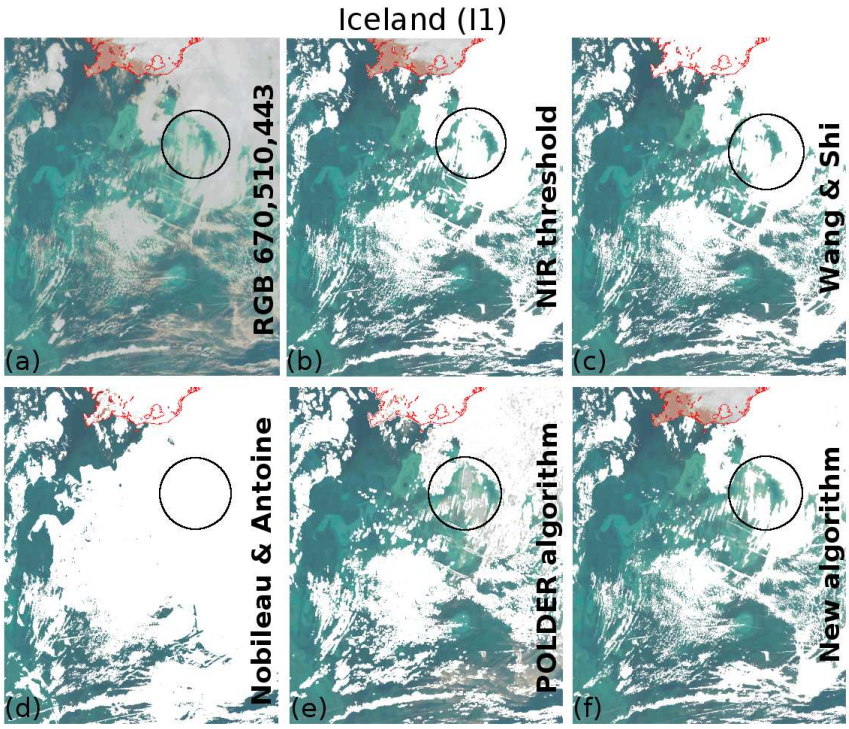

Fig. 7. As Fig. 4 but for scene I1.

To test how much data is gained when using our algorithm instead of the SeaWiFS NIR threshold and the algorithm by Wang and Shi, the number of pixels classed as water by the three methods is compared in several scenes from the regions described above (Fig. 1). In the regions A, R, Y and scenes E1 and E2 where the SeaWiFS NIR threshold masks a lot of water as clouds, the gain of data is high. In the other regions, where the NIR threshold works relatively well, the gain is considerably lower (table 1).

Table 1. Examples of the increase in the number of water pixels when using the algorithm instead of the standard SeaWiFS NIR threshold and the algorithm by Wang and Shi [4]. The regions correspond exactly to those in Fig. 1.

		Gain [%]				Gain [%]	
Scene	Date	vs NIR threshold	vs Wang & Shi	Scene	Date	vs NIR threshold	vs Wang & Shi
A1	2003-08-15	34.3	13.8	E5	2004-06-15	2.54	2.11
A2	2003-08-25	34.0	23.5	R1	2001-07-29	18.5	3.27
A3	2003-09-15	21.6	7.64	R2	2002-01-08	9.87	2.05
A4	2003-09-30	7.57	21.2	R3	2002-08-26	19.3	9.20
A5	2003-11-03	41.1	20.5	R4	2003-05-26	20.0	5.89
A6	2003-12-16	43.9	22.8	R5	2004-03-13	38.9	20.5
E1	2004-01-11	10.8	8.17	R6	2005-10-02	10.4	2.44
E2	2004-01-18	10.9	9.26	Y1	2001-03-30	63.3	21.3
E3	2004-03-02	3.01	1.68	Y2	2004-11-12	48.1	26.3
E4	2004-06-07	3.92	-1.75	I1	1998-06-15	4.72	2.84

#107421 - $15.00 USD Received 10 Feb 2009; revised 8 May 2009; accepted 19 May 2009; published 6 Jul 2009

3.2 Sensitivity analysis

First, the impact of the cloud optical thickness on the ρ_s spectral variability, Eq. (7), is assessed by numerical simulations, with settings and input as described in Sec. 2.3. As expected, the simulated reflectance spectra show that the spectral dependence decreases with increasing optical thickness (Fig. 8(a)). In this case the detection limit is around $\tau(555)=1.0$, since this gives an ε_{max} just below the threshold value 2.5. Therefore, a cloudy pixel with optical thickness lower than 1 (albedo of 5%) will be classed as water or mixed, for this type of highly turbid water. The marine reflectance spectrum used in the simulations has a high signal in the NIR due to the high concentration of suspended matter (180 mg/l), and would be classed as a cloud by the standard SeaWiFS NIR threshold also when the atmosphere is clear. Note that this spectrum represents a situation where cloud detection is difficult with our algorithm: the high marine reflectance will constitute a large part of the TOA reflectance and the signal measured by the satellite will show a high spectral variability compared to a case with less sediment-rich water, especially for thin clouds. A lower detection limit can therefore be expected in less turbid cases. Specific studies should be performed in order to estimate the marine reflectance of turbid waters under a thin or broken cloud layer, as it has been done for open ocean waters [5].

A second set of simulations shows that the effect of variations in cloud altitude on ρ_s is very small (Fig. 8(b)). For a cloud with $\tau(555)=5.0$, a change in cloud altitude from 0.5 km to 2.5 km causes a change of 1.1% in the mean ρ_s in a wavelength interval from 400 to 420 nm. The effect is even smaller at longer wavelengths and for smaller optical thicknesses.

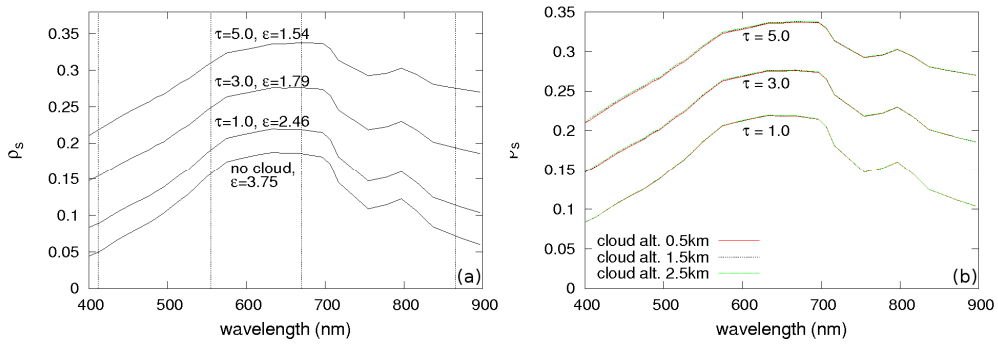

Fig. 8. (a). ρ_s simulated for a stratocumulus cloud of different optical thickness $\tau(555)$. The cloud altitude is 1.5 km and the wind speed 5.0 m/s. The ratio ε_{max} is indicated for each spectrum. (b) ρ_s simulated for three different cloud altitudes, 0.5, 1.5 and 2.5 km, and for three different cloud optical thicknesses, $\tau(555)=1.0$, 3.0 and 5.0.

4. Concluding remarks

Different algorithms for cloud detection have been tested in 20 SeaWiFS images from five geographic regions with different types of Case-2 waters. An algorithm based on the lower spectral variability of clouds compared to water has been developed and tested. It shows a good overall performance compared with the other algorithms, and an ability to recover a higher number of marine pixels in turbid Case-2 waters that would otherwise be considered as clouds and subsequently masked. Examination of training pixels from the different scenes (Fig. 2(a)), visual inspection of the images using different color composites, and a sensitivity analysis based on numerical simulations suggest that the algorithm is capable of detecting clouds, also with low optical thickness. The detection limit was found to be $\tau(555)=1.0$ for an

#107421 - $15.00 USD Received 10 Feb 2009; revised 8 May 2009; accepted 19 May 2009; published 6 Jul 2009

SPM concentration of 180 mg/l (Fig. 8(a)). Thin or broken clouds, especially over very turbid waters, are often close to the threshold and thus difficult to identify. One way to deal with this is to introduce a third class for such pixels and leave them unidentified. The algorithm is developed for turbid Case-2 waters, and its ability to detect thin clouds over Case-1 waters has not been closely investigateded. Some of the gain in the number of water pixels (Table 1) when using our algorithm is due to undetected clouds, as can be seen in a scene south of Iceland (Fig. 7(f)). Scenes from the same geographic areas, but different pixels, have been used both for the development and the tests of the algorithm, and further tests should be made to ensure its robustness. However, a large range of optical properties has been covered in this study. The most difficult of the tested regions appeared to be the east coast of China, where the reflectance spectra are relatively flat, certainly due to a strong contribution from aerosols in the blue wavelengths.

Acknowledgments

This work was founded by Centre National d'Étude Spatiale in the frame of the TOSCA program (COULCOT project). SeaWiFS images are provided by NASA Goddard Space Flight Center. We thank Nicolas Henriot for information about the POLDER/PARASOL cloud mask, and David Doxaran for the reflectance spectra used in the numerical simulations. The authors thank three anonymous reviewers for their relevant comments.

#107421 - $15.00 USD Received 10 Feb 2009; revised 8 May 2009; accepted 19 May 2009; published 6 Jul 2009